15th AIAA/CEAS Aeroacoustics Conference (30th AIAA Aeroacoustics Conference)
11 - 13 May 2009, Miami, Florida

AIAA 2009-3190

Numerical Modeling of Plasma Actuators in High Speed Jets

Randall R. Kleinman,* Daniel J. Bodony† and Jonathan B. Freund‡
University of Illinois at Urbana-Champaign, Urbana, 61801, USA

Localized arc-filament plasma actuators (LAFPA) have been demonstrated to have the control authority needed to fundamentally alter the development of supersonic turbulent jets and suppress their noise. Fundamentally, these actuators are thought to work via a Joule heating by the plasma, causing locally hot regions of fluid, but the mechanism by which this affects the instabilities of the jet is unknown. A simulation model of the near-nozzle region of an actuated jet is used to investigate this. The model matches the jet Reynolds number of corresponding experiments at The Ohio State University (OSU), which is important because the boundary layer interaction with the plasma actuator is expected to be central to the mechanisms. The model is also limited in that it is two dimensional, so direct correspondence with the experiments is not expected. However, it does include what are thought to be the key features of the flow: a localized rapid heating, a recessed groove in which the plasma sits, a thin boundary layer, and the early development and saturation of instabilities in the shear layers. It also matches some observations from the experiment. With the simulations, we show that the geometry of the groove, which was originally designed to prevent the plasma from being "blown off" by the flow, is of central importance for the actuation. The rapid expansion resulting from the heating causes an ejection of fluid from this cavity perpendicular to the shear layer that forms over it. Numerical experiments using reduced models of the actuator are designed to assess the respective role of the the cavity, the vertical ejection of fluid from the cavity, and the direct effect of thermal actuation on the flow. An actuator placed above the nozzle wall without a cavity is shown to have little effect on the flow. None of the reduced models match the mixing layer spreading or the flow organization caused by the the full actuator.

I. Introduction

Plasma actuation of different types are being considered for various flow control objectives. Dielectric barrier discharge (DBD),[1] DC and RF glow discharge,[2,3] and arc-filament discharge[4–6] plasmas are all being actively researched for applications in boundary layer separation control, shock wave control, noise mitigation, and shear-flow mixing enhancement. The primary mechanisms by which these types of plasmas interact with the flow make each type better suited for different control objectives in different flow regimes. For example, DBD-based actuators produce electrohydrodynamic interactions by accelerating charged molecules via a Coulomb force and in that way can locally accelerate a flow. This technology has been used effectively for boundary layer separation control in airfoils.[7] However, it does not seem that DBD actuators have sufficient authority to force high-speed (near-sonic or above) flows such as a jet,[8] which is our current control objective. Arc-filament discharge actuators appear to be the best suited to this case. They are thought to generate pressure perturbations via rapid Joule heating in the ionized gas they establish in their vicinity. This heating has been shown to be strong enough to produce shock waves and flow separation in supersonic boundary layers.[9] They have also demonstrated the capability to excite stongly amplified

*Theoretical and Applied Mechanics Degree Candidate, Mechanical Science & Engineering, University of Illinois at Urbana-Champaign, and AIAA Student Member
†Assistant Professor, Aerospace Engineering, University of Illinois at Urbana-Champaign, and AIAA Member.
‡Associate Professor, Mechanical Science & Engineering and Aerospace Engineering, University of Illinois at Urbana-Champaign, and AIAA Senior Member.

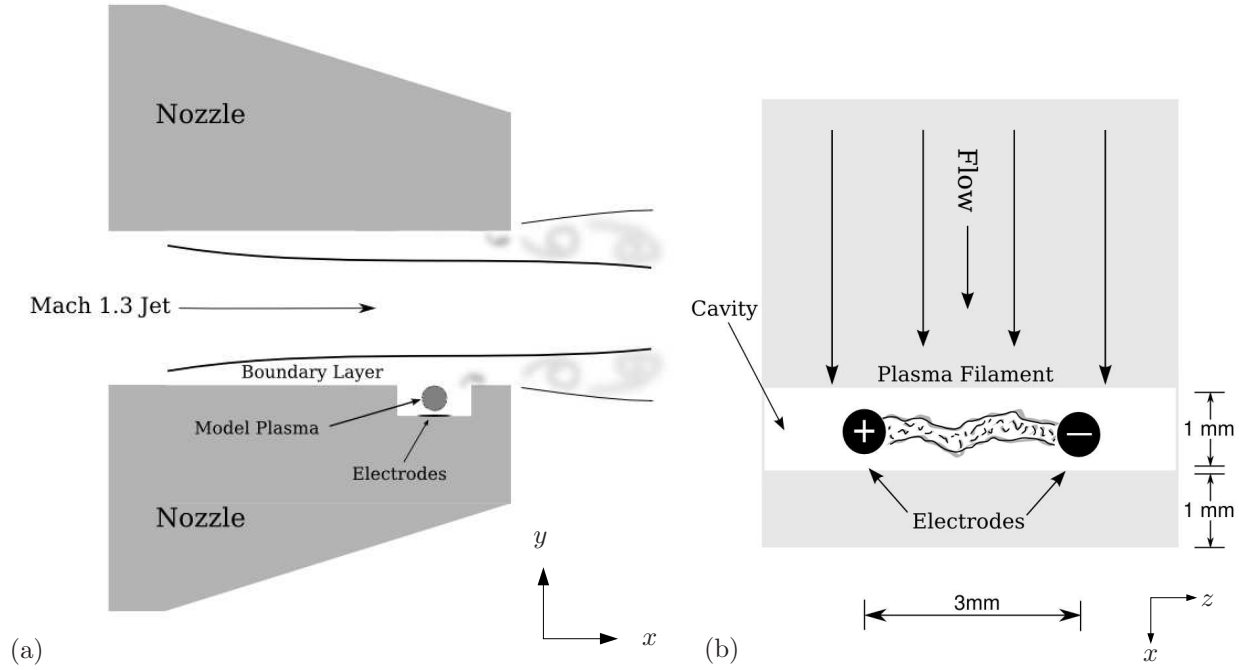

Figure 1. Drawings of the OSU Mach 1.3 jet nozzle exit and plasma actuator cavity geometry. (a) Side view of the nozzle exit showing the cavity in the near-nozzle exit region of the jet where the actuator model is implemented. (b) Top view (from inside nozzle) of the cavity showing the actuator electrodes and arc-filament plasma within cavity.

instabilities in high-speed jets,[6] making them a promising technology in aeroacoustic control and jet noise reduction.

The specific localized arc-filament plasma actuators (LAFPA) we consider are currently under continued development at The Ohio State University (OSU) by Professor M. Samimy and colleagues with the intent of controlling sub- and supersonic jets[6] and cavity flows.[10] Recent work reporting the development and characterization of LAFPA has shown that they offer significant control authority over fluidic-based actuators (*e.g.* synthetic jets) with the further advantage of having no moving parts. By targeting the instabilities in a jet, power requirements are relatively low, around 20 Watts average power each in laboratory jet experiments. LAFPA also have the advantage of being able to force at a wide range of frequencies: from a few kHz up to 200 kHz. This flexiblity and high control authority makes them potentially useful in a wide range of applications. Depending on the forcing applied, the actuators have increased downstream mixing[6] and reduced far-field noise relative to an unforced baseline jet.[11]

These successful demonstrations are highly encouraging, but the detailed mechanism by which the LAFPA act on a flow is still unclear. It is therefore also unclear how they might be designed and used most effectively. The generated plasma is known to quickly create a local high-temperature region, which is thought to be the root forcing mechanism. What is not known is how this thermal source (an 'entropy mode' in a linear sense) alters the flow and drives the observed downstream response ('vorticity mode') in the initial shear layers of a jet. The local geometry in the neighborhood of the plasma arc might be important in this. In the OSU jet experiments the array of electrode pairs that create the plasma is recessed in a rectangular cross section cavity near the nozzle outlet (Fig. 1). This cavity forms a ring-shaped groove around the inner circumference of the jet nozzle. It was added to stabilize the plasma by shielding it from the nozzle boundary layer flow, which was observed to advect the plasma away from the electrodes, causing it to breakdown.[4] It remains unclear what, if any, effect the cavity has on the interaction between the arc-filament discharge and the flow.

Experimental diagnostics of the actuation are difficult due to interference emitted by the plasma, the relatively small dimensions of the nozzle exit region, and the harsh environment in which the LAFPA system operates. We have therefore designed a high-fidelity simulation model to identify the important mechanisms leading to excitation of the flow downstream. This will facilitate future optimization and effective use of the LAFPA technology in a range of flow control applications, especially jet noise control. Specifically, we

have developed a numerical model of the plasma and implemented it in a high-fidelity compressible flow solver that includes the cavity and the near-nozzle shear layer of the jet. Our simulations of the near-nozzle region of a Ma = 1.3 jet match the actuator geometry and the Reynolds number based upon the boundary layer momentum thickness. However, at present the model is two dimensional; a more realistic fullly three-dimensional simulation at the jet Reynolds number is prohibitively expensive. However, the key features of the flow are represented: the injection of thermal energy due to the plasma, the cavity, the nozzle lip, and the early development of the shear layer. Validation against multiple experimental observations support this. Variation of the forcing parameters is then used to study the detailed mechanisms of the actuation.

II. LAFPA for Jet Control: Background

The LAFPA system is implemented on a high-speed and high-Reynolds-number jet in ongoing experiments at OSU. Relevent details of the flow facility and experimental conditions are described briefly here. A full description is provided by Samimy *et al.*[6] The standard experiments consist of a Mach 1.3 axisymmetric jet with a Reynolds number of $Re_{\mathrm{D}} = 1.1 \times 10^6$ based on the jet exit diameter $D_{\mathrm{j}} = 2.54$ cm and the jet centerline velocity. The jet is operated as near to an ideally expanded condition as possible.

A boron nitride nozzle extension attached to the end of the nozzle houses the plasma actuators as shown schematically in Fig. 1(a). A rectangular cross section groove of width $L_{\mathrm{c}} = 1$ mm and depth $D_{\mathrm{c}} = 0.5$ mm is machined in the nozzle extension 1 mm upstream of the exit. The plasma is generated between two high-voltage steel or tungsten pin electrodes spaced 3 mm apart in the bottom of the groove as seen in Fig. 1(b). Visual observation confirms that the plasma glow is always located inside the cavity. In laboratory experiments, eight such pairs of electrodes are evenly spaced along the circumference of the nozzle extension in the ring groove.

The actuation is created using a high-voltage plasma generation system developed at OSU to enable simultaneous operation of up to eight actuators with independently variable frequency, duty cycle, and phase. The time dependence of a pulse is approximately a square wave, so only its fraction of time 'on' (its duty cycle) can be set. The current is limited to 250 mA, so by multiplying by the voltage difference across the electodes the maximum power is 100 W while the actuator is on. The time-averaged power depends on the specified duty cycle.

III. Methods

III.A. Plasma Heating Model

Numerical models of several different plasmas have been formulated using a combined Navier-Stokes/Maxwell equations approach.[12] In many cases, these models are quite involved due to the complexity of the underlying plasma physics. However, the principal effect of the present arc discharge is thought to be a localized heating, which we can model simply as a time-varying, spatially-distributed source of internal energy. A similar approach was followed in the one-dimensional model of Utkin *et al.*[5] In their work, an axisymmetric compressible Navier-Stokes simulation with a cylindrical heating power source was used to estimate the pressure and temperature fields due to the plasma filament, neglecting any effects of the cavity. We have extended the this cylindrical power source model to two dimensions and incorporated it into direct numerical simulations of the flow.

Our model is parameterized based on the available experimental data for these specific actuators.[4–6,13] The plasma is assumed to be a cylindrical heat source with length $L_{\mathrm{act}} = 3$ mm and a radius of $r_0 = 0.25$ mm based on the spacing of the electrodes and observations of the plasma. The thermal source added to the governing energy equation is

$$S_{\mathrm{act}}(r(x,y),t) = w(t)\frac{f(r(x,y))}{f_{\mathrm{V}}}\frac{P_{\mathrm{act}}}{\pi r_0^2 L_{\mathrm{act}}}, \tag{1}$$

where the spatial distribution is

$$f(r(x,y)) = \frac{1}{2}\left[\tanh\left(-\sigma_{\mathrm{xy}}\left(r(x,y) - \frac{2}{3}r_0\right)\right) + 1\right] \tag{2}$$

and $r(x,y) = \sqrt{(x - x_{\mathrm{act}})^2 + (y - y_{\mathrm{act}})^2}$ with x and y the streamwise and cross-stream coordinates as shown in Fig. 1. The source is centered at $(x_{\mathrm{act}}, y_{\mathrm{act}})$, which is set to be the geometric center of the cavity. The

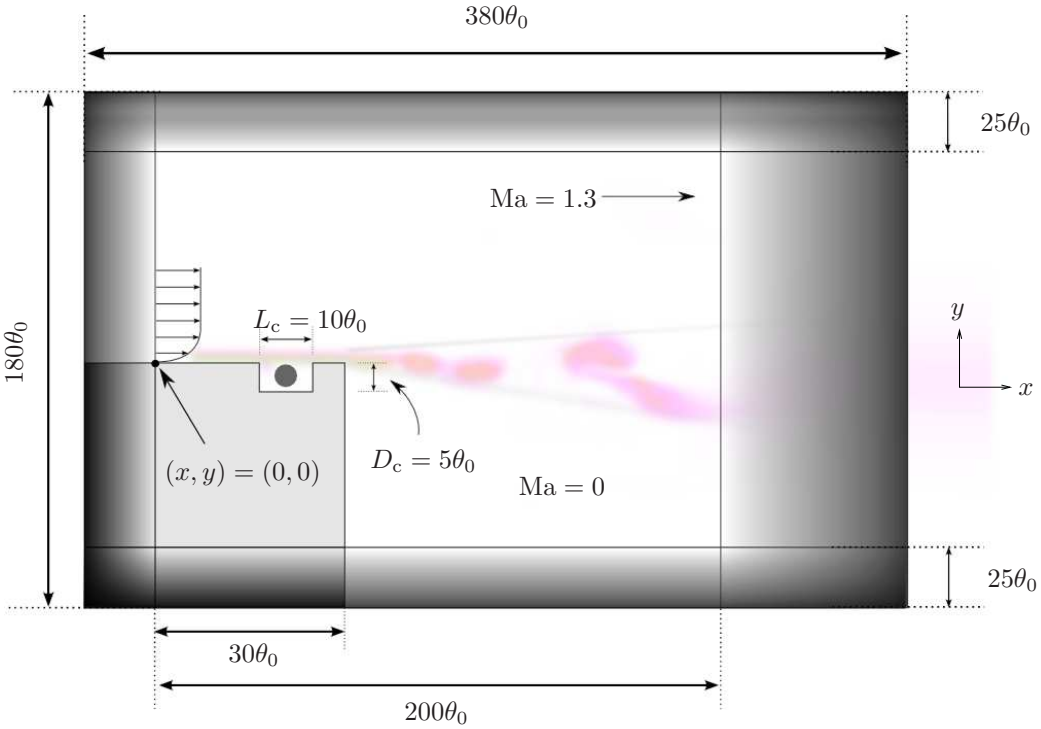

Figure 2. Schematic of the computational domain of the direct numerical simulations. Dimensions are presented in terms of the momentum thickness at the nozzle exit, θ_0. The light grey area denotes computational space treated as a solid, isothermal wall. The shaded area on all four sides of the domain denotes the computational boundary (buffer) zones. The black circle located in the cavity shows the location of the internal energy source term in Eq. (1). Note: dimensions are not to scale.

parameter $\sigma_{xy} = 10/r_0$ controls the sharpness of the model's distribution function. The power imparted to the flow by the plasma $P_{act} = 100$ W is divided by the volume of the 3 mm long cylinder, as it would be in three dimensions, for dimensional consistency in the energy equation. The constant

$$f_V = \int_0^\infty f(r)\mathrm{d}r \tag{3}$$

ensures that the spatial distribution does not provide additional energy to the heat source.

The time-varying portion of the source term models the square-wave input signal as

$$w(t) = \frac{1}{2}\left[\tanh\left(\frac{t - t_i}{t_r}\right) - \tanh\left(\frac{t - t_f}{t_r}\right)\right]. \tag{4}$$

The constants are as follows: $t_r = 1\ \mu s$ is the rise time of the actuator signal determined by the power supply, $t_i = 10\ \mu s * f_{act}$ is the delay of the actuator signal, and $t_f = t_i + p_{dc}T_{act}$ governs the actuator 'off' time and is based on the duty cycle p_{dc}. In the simulations presented in this work, only the duty cycle is varied.

III.B. Flow Domain and Parameters

The numerical plasma model of the previous section is incorporated as an internal energy source term into direct numerical simulations of the compressible Navier-Stokes equations in two dimensions. No modeling is used in the fluid flow solution. The equations are nondimensionalized by the speed of sound $c_\infty = 343$ m/s, density $\rho_\infty = 1.2$ kg/m^3, viscosity $\mu_\infty = 1.87\times10^{-5}$ kg/(m·s), temperature $T_\infty = 300$ K, and the momentum thickness at the exit of the experimental jet $\theta_0 = 0.1$ mm. Based on these values, the momentum thickness Reynolds number is $\mathrm{Re} = 3330$, which matches the experimental jet Reynolds number. The Prandtl number is $\mathrm{Pr} = 0.7$. Despite some loss of accruacy due to the locally high temperatures near the actuator, the ideal gas equation is used to close the system of equations.

The simulation domain covering the near-nozzle region of the OSU experimental jet is shown schematically in Fig. 2. The basic flow is a $\mathrm{Ma} = 1.3$ compressible boundary layer above a solid (no slip) wall located

at $y = 0$ with fixed wall temperature $T_w = T_\infty$. There is no flow (Ma = 0) downstream of the nozzle exit for $y \ll 0$. All wall boundaries are isothermal. With the inclusion of the thermal source, some amount of heat transfer from the cavity fluid to the boron nitride nozzle extension is expected, but we do not model this beyond recognizing that the thermal conducitivy of the nozzle is high and that the acuators are small thermal sources. An isothermal model of the actuator cavity is therefore expected to be reasonably accurate.

The laminar inflow boundary layer is specified above the wall using the method outlined by Lui.[14] The actual boundary layer leaving the nozzle lip at these condutions is too thin to accurately measure its profile. Estimates from experiments using a nozzle with similar length but at different flow conditions suggest[15] that the boundary layer is turbulent with a momentum thickness of around $\theta = 0.1$ mm, but there is also some evidence that it may actually be laminar. Based on the acceleration parameter $K = \nu/U^2 \partial U/\partial x$ employed by Viswanathan and Clark[16] and a RANS solution of the jet mean flow gradient near the nozzle, the boundary layer in this flow is expected to be laminar. Regardless, a laminar boundary layer is used in this investigation of mechanisms. The non-dimensional momentum thickness of the layer (θ/θ_0) was specified to be equal to unity at the nozzle exit ($x = 30\theta_0$ in Fig. 2). The downstream simulation domain extends to $x = 200\theta_0$ so that we can study the near-'nozzle' response of the shear layers. The cross-stream domain extends out to $y = \pm 65\theta_0$. For reference, in terms of the experimental jet dimensions the streamwise domain extends to about $x = 0.8D_j$ and the cross-stream domain from $y = \pm 0.25D_j$.

III.C. Numerical Methods

A full description of the numerical schemes is given elsewhere[17] and only briefly outlined here. The flow equations are solved using high-resolution explicit and compact finite difference schemes and fourth-order Runge–Kutta time integration. The streamwise differencing scheme is a sixth-order variant of the dispersion-relation-preserving scheme of Tam and Webb.[18] The cross-stream scheme is the fourth-order 'spectral-like' pentadiagonal compact finite-difference scheme of Lele.[19] Both of these schemes have stencils that could support higher-order schemes based upon their truncation error, but instead have coefficients optimized for higher resolution for fixed mesh size. A standard sixth-order explicit scheme is used for second derivatives in both coordinate directions. Fourth-order biased schemes are used at the walls and the edges of the computational domain. The mesh is Cartesian and stretched so as to cluster points in the cavity and shear layer. The mesh size was $N_x \times N_y = 3000 \times 1001$, and the numerical time step was $\Delta t c_\infty/\theta_0 = 0.005$.

The Navier–Stokes characteristic boundary conditions[20] with the viscous correction of Yoo and Im[21] applied are used for boundary conditions on the isothermal walls. One-dimensional characteristics are used on the computational domain edges. Fig. 2 shows shaded areas indicating the boundary 'buffer zones'. This type of boundary treatment is common in aeroacoustic simulations for accurately absorbing outgoing disturbances.[22] Low-order, low-pass filtering is also implemented in these zones to reduce any numerical artifacts generated at these outer boundaries. Lastly, numerical stabilization of the flow solutions is provided by high-order, high-wavenumber filtering in the physical domain of the solution.[19] The flow solution is filtered in both coordinate directions every five time steps. A linear combination of the filtered solution (40%) is combined with the unfiltered solution (60%) at that time step and taken as the new simulation solution. The filtering is purely for numerical stabilization and is confirmed not to alter the physical behavior of the flow.[17] The present results were also confirmed to be mesh independent.

III.D. Actuator Forcing Parameters

The simulations incorporating the actuator model in this work are performed with a forcing frequency of 20 kHz. This frequency was chosen because experiments showed the development of actuation-induced perturbations at this frequency occurred closer to the nozzle exit than lower frequencies and were stronger in general (see Samimy, *et al.*, figure 4).[6] The perturbations also decayed quickly downstream and therefore 20 kHz forcing allowed for the strongest mixing layer response to be captured in the small computational domain. Settings of 5%, 10% and 20% duty cycle are presented in this paper. For 10% duty cycle, the actuator is 'on' for 5 μs of the actuator's $T_{act} = 50\mu s$ period. Using these forcing parameters, the time series (Eq. 4) and the corresponding frequency spectra of the forcing are shown in Fig. 3.

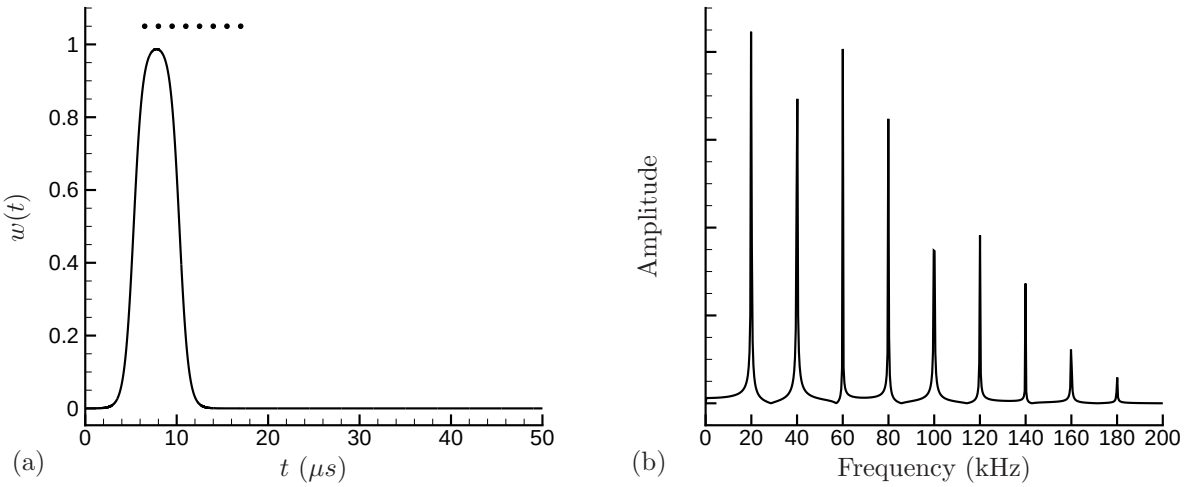

Figure 3. (a) Time series of $w(t)$ for 20 kHz forcing with 10% duty cycle for one actuation period. (b) Corresponding frequency spectrum of $w(t)$ showing the 20 kHz forcing frequency and harmonics.

IV. Results and Discussion

Results of the simulations are presented in this section beginning with validation of the model. We first focus on the region of the actuator to understand the mechanism by which the flow is affected by it. Then, we examine the subsequent downstream growth of the shear layer including frequency spectra resulting from the actuated cases.

Each simulation presented here is advanced in time from the initial condition for one-million time steps to allow for initial flow transients to convect out of the domain. The actuator is active during this initial simulation. Statistical data is then collected during the following two-million time steps. This corresponds to 33 domain flow-through times (based on the shear layer convection velocity of $0.65\Delta U$) and 58 actuator forcing periods. Phase-averaged quantities presented below are averaged over all of these 58 forcing periods.

IV.A. Model Validation

As mentioned in the Introduction, detailed experimental characterization of the cavity and near-nozzle region is limited for several reasons. However, there do exist two convenient points of comparision with the experiments to assess whether or not the simulations are at least qualitatively in line with the actuators in the experiment. Estimates are available of the temperature of the plasma in the cavity and the sound pressure level (SPL) at a location slightly downstream of the nozzle exit.

IV.A.1. Pressure

The pressure amplitude for the ideally expanded Mach 1.3 jet of the OSU experiments is compared with the results of the simulations presented here. The actuation was axisymmetric (i.e. all actuators firing simultaneously) for a 20kHz forcing with a 20% duty cycle. The pressure measurement was made at a location where the probe just grazed the edge of the shear layer, half a jet diameter downstream ($x/D_\mathrm{j} = 0.5$) of the nozzle lip. This corresponds in the simulation to $(x, y) = (127, 20)\theta_0$. The experiments report an amplitude of 172 dB at $x/D_\mathrm{j} = 0.5$ but the trend shows the amplitude decreasing sharply afterwards, suggesting a higher reading closer to the nozzle. The corresponding computed SPL is 173 dB, which is in reasonable agreement with the experiment.

Figure 4(a) shows the SPL along the streamwise coordinate (x) at the nozzle lip ($y = 0$). This location is within the shear layer at all streamwise locations and is therefore expected to have a higher perturbation amplitude than the experiments for this region close to the nozzle exit. At 20 kHz forcing, the simulation and actuator model correctly capture the pressure perturbations saturating shortly downstream of the nozzle exit, but the computational domain ends before any decrease can be seen.

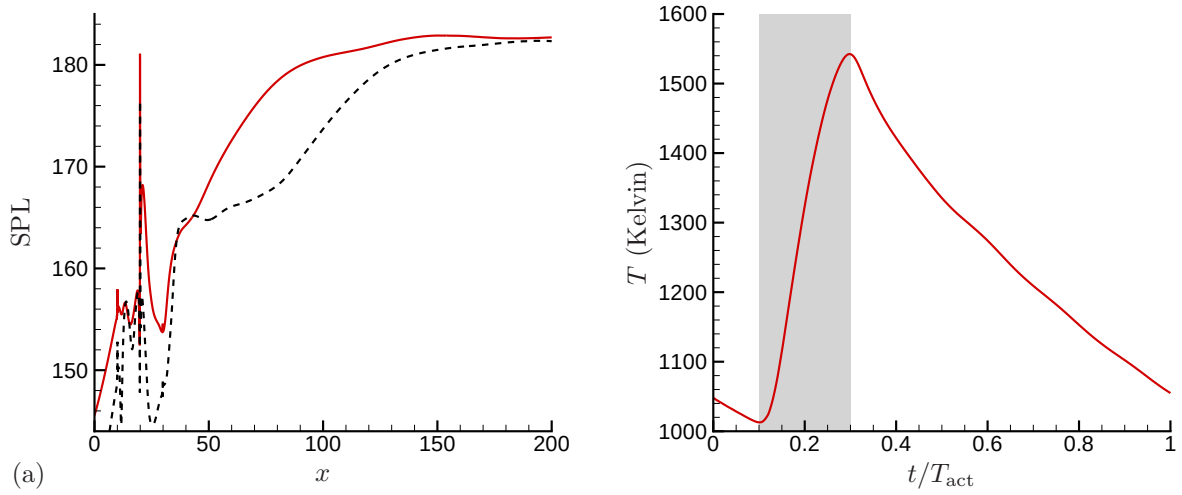

Figure 4. (a) Sound pressure level of the cavity simulation (———) and baseline (no actuation, – – – –) simulation at the lipline ($y = 0$) as a function of streamwise distance. (b) Phase-averaged maximum temperature in the cavity for 20kHz forcing and 20% duty cycle. The shaded region denotes the time where the actuator model is "on".

IV.A.2. Temperature

The second model validation comes from comparing the reported plasma temperature and the maximum temperature of the fluid in the model simulations. The temperature in the experiments is calculated from emission spectroscopy since it was not feasible to measure with probes. A least-squares fit was used to compare the measured spectrum and the synthetic spectra from the second positive band system of nitrogen calculated numerically using temperature as a free parameter. Results of this calculation suggest that the plasma reaches temperatures near 2000 K,[23] although depending on the type of power supply the temperature could be as low as 1200 K.[13] The one-dimensional model of Utkin *et al.*[5] also shows a maximum temperature near 2000 K. The maximum temperature in the cavity for the current model is shown in Fig. 4(b). The phase-averaged temperature in the cavity for 20 kHz forcing at 20% duty cycle is shown to have a maximum temperature of around 1550 K. When the temperature is not phase-averaged, the maximum temperatures of the fluid in the groove do reach slightly over 1800 K at times. Overall, this seemed to be a reasonable agreement.

IV.B. Cavity Region Visualization

Visualizations of the velocity vector fields in Figs. 5(a)–(h) show a recirculation region in the cavity, as might be expected for any cavity of this aspect ratio. This recirculation is driven, in a sense, by the shear layer above the cavity, which forms at the upstream edge where the upstream boundary layer detaches. As the actuator turns on, starting at $t = 5$ μs (see Fig. 3a), the upward fluid motion in the middle of the cavity, which is the upward part of the this recirculating flow, appears to be accentuated. By $t = 9.5$ μs (Fig. 5c), high-speed fluid is starting to also be ejected from the downstream edge of the cavity in a kind of jetting motion. At $t = 12.5$ μs (Fig. 5e), this ejected fluid has a vertical velocity component that is a significant fraction of its horizontal component. Because of the thermal input from the actuator over several cycles, the fluid ejected from the cavity is hot and therefore can be clearly seen in visualizations of the temperature field in Figs. 5(i)–(l). Despite obvious stretching and deformation of this ejected fluid by the boundary layer, by $t = 14$ μs (Fig. 5l) there is nearly θ_0 thick layer of hot fluid on the wall just downstream of the cavity.

This ejection suggests that at least part of the actuator's forcing mechanism appears to be like a fluidic actuator, such as a synthetic jet but driven by a thermal expansion rather than a mechanical wall motion. We therefore can anticipate that if the actuator were more confined, as in a narrower cavity, a stronger ejection might be formed by the thermal expansion. This was tested by decreasing L_c from $10\theta_0$ down to $5\theta_0$, making it one-half the width of the OSU actuators. This cavity now essentialy matches the width of the model plasma thermal source. Velocity visualizations of this narrow-cavity actuator are shown in

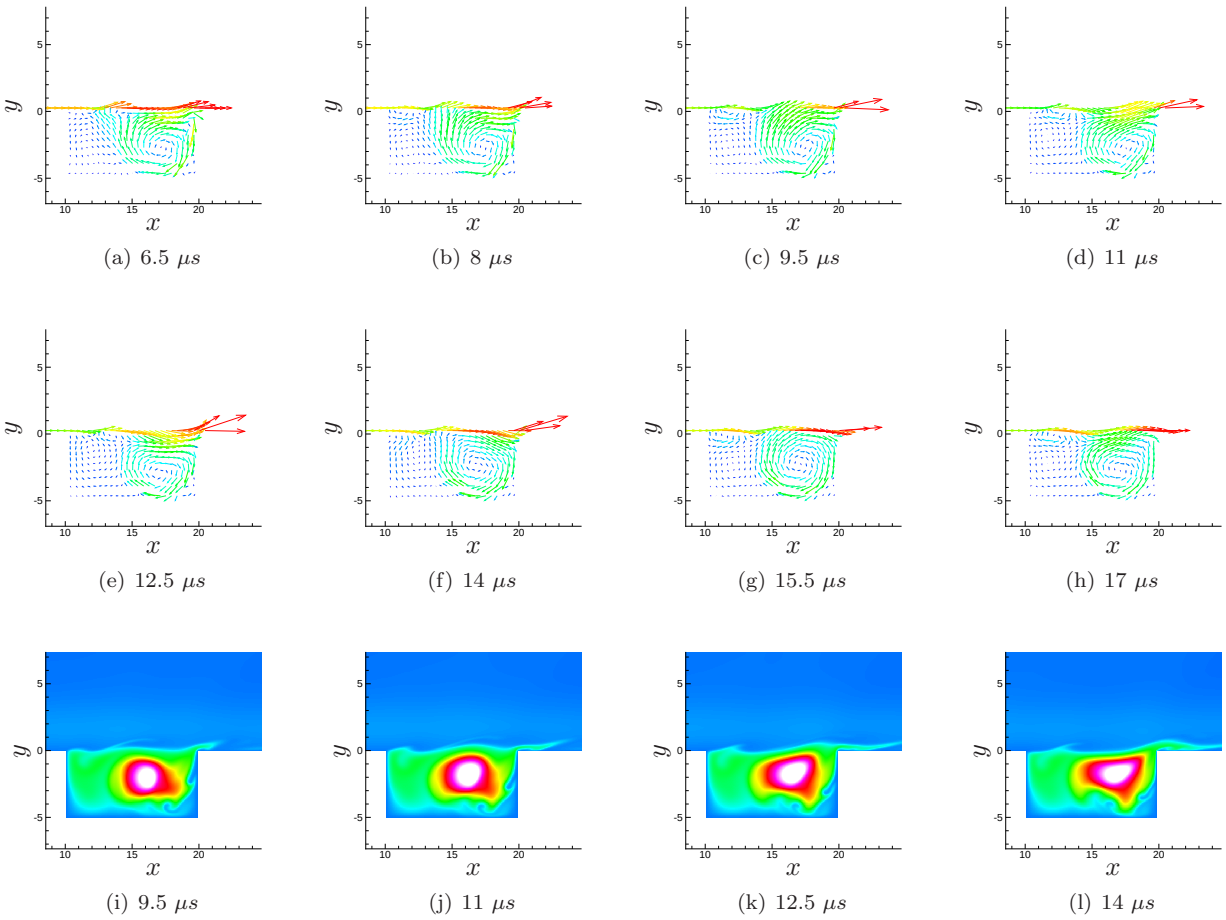

Figure 5. (a-h) A time series of the velocity vector field of the cavity during actuation. Each vector's length is proportional to its magnitude. For reference, the dots in Fig. 3(a) mark the times in the forcing period which correspond to the vector fields shown. The time listed below each figure is the time after the beginning of the period of actuation. (i-l) Temperature fields of the cavity region for a subset of the period of actuation corresponding to the vector fields in (c)–(f).

Fig. 6. The recirculation in this case is now centered in the cavity. When the actuator is not firing (e.g. Fig. 6h), there are no obvious instabilities seen in the velocity field of the detached shear layer of the kind that were evident for the wider cavity (e.g. Fig. 5h), presumably because there is less distance for the growth of Kelvin-Helmholtz modes in this smaller cavity case. However, when the actuator turns on (e.g. Fig. 6c) there is an even more prominent expulsion of fluid from the downstream edge of the cavity. If this jetting is important for the downstream evolution of the shear layer, we expect there to be a stronger response for this narrower cavity.

The amount of fluid mass expelled from the cavity when the actuator activates is shown in Fig. 7(a) for both the $L_c = 10\theta_0$ and $L_c = 5\theta_0$ cavities. Nearly the same amount of mass is expelled in both cases, peaking just after the end of the period of activation of the actuator. The visualizations show that this ejection is also more focused by the narrower geometry of the cavity. The subsequent oscillations are the natural instabilities of the cavity and coincide with the well-known Rossiter modes.[24,25] Using Rossiter's semi-empirical formula, the cavity oscillation frequency for the parameters of this flow is roughly 132 kHz. An estimation from Fig. 7(a) points to an oscillation frequency of 135 kHz. This cavity frequency is not significant in the spectra of the downstream flow region (see section IV.D). The wider cavity has significantly stronger fluctuations, presumably because the instabilities can amplify to high levels by the end of the cavity.

Changing the duty cycle of the actuation only weakly affects the peak mass ejection. Ejected mass fluxes for the wider ($L_c = 10\theta_0$) cavity are shown in Fig. 7(b) for 5%, 10% and 20% duty cycles. There is some more mass ejected for the longer actuator on-times, but switching from 5% to 10% changes the overall mass ejection relatively little. At 20% duty cycle, it seems that the ejection interacts with the instabilities excited

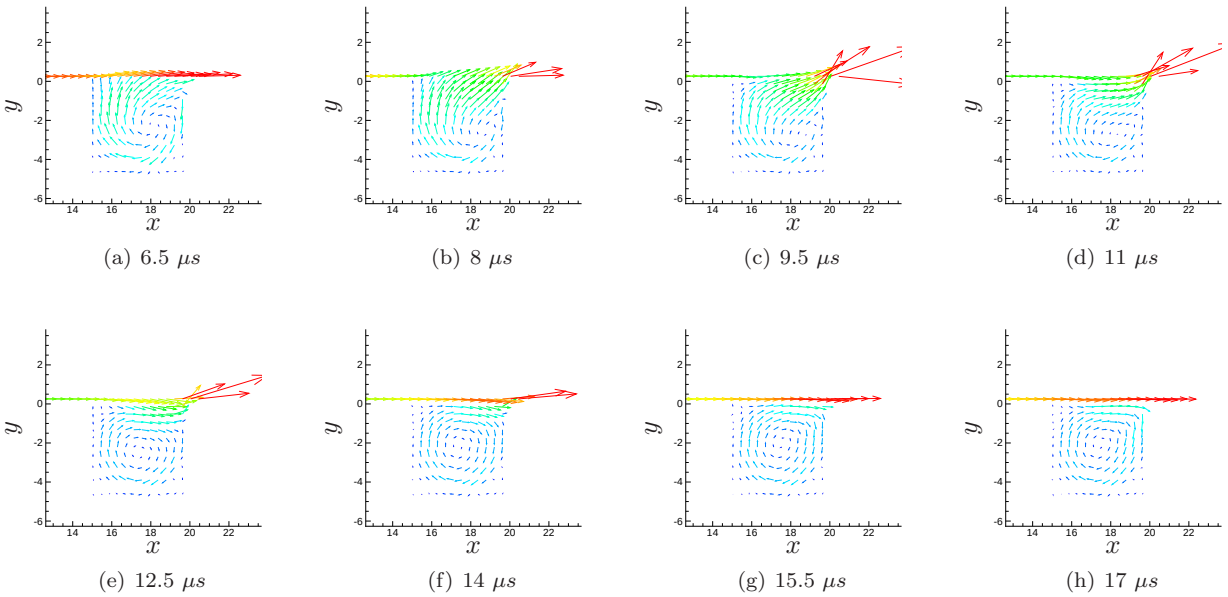

(a) 6.5 μs (b) 8 μs (c) 9.5 μs (d) 11 μs

(e) 12.5 μs (f) 14 μs (g) 15.5 μs (h) 17 μs

Figure 6. A time series of the velocity vector field of the narrow cavity ($L_c = 5\theta_0$ width) during actuation. Each vector's length is proportional to its magnitude. For reference, the dots in Fig. 3(a) mark the times in the forcing period that correspond to the vector fields shown.

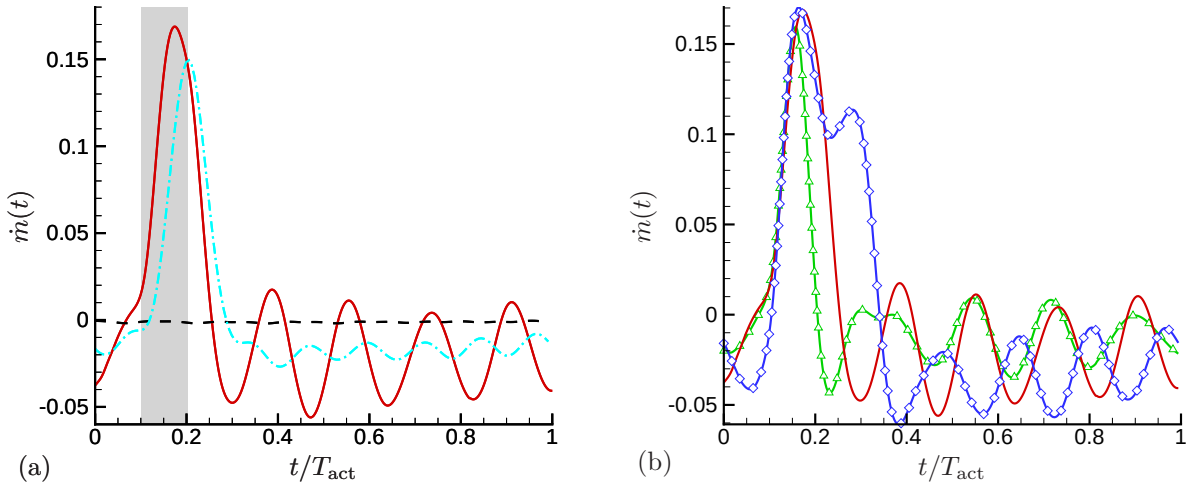

Figure 7. (a) Mass flux (per unit depth) out of the cavity calculated at $y = 0$ of the baseline (– – – –), $L_c = 10\theta_0$ (———), and $L_c = 5\theta_0$ (—·—·—) cavities phase averaged over the forcing frequency. The grey region indicates the time the actuator was turned 'on'. (b) Mass flux (per unit depth) as in (a) but for three different duty cycles for the $L_c = 10\theta_0$ cavity: 5% (– △ –), 10% (———), and 20% (– ◇ –).

by the Rossiter mode, giving the principal ejection another "bump" and putting the subsequent Rossiter oscillation 180° out of phase with those for the lower duty cycle cases.

IV.C. Downstream Layer Growth

While it is clear from the OSU experiments that the actuators are indeed effective at exciting the jet shear layers, the precise mechanisms of this are difficult to antitipate. As discussed above, the prinicipal effect of the actuator is thought to be thermal heating, so this is really a question of how this thermal source comes to alter the vortical development of the shear layer. A baroclinic torque is an obvious candidate,

wherein non-parallel pressure and density gradients, for example, can lead to the generation of vorticity and presumably thereby the vortical structures seen in the mixing layer. Investigations of this mechanism are currently underway. However, the apparent jetting from the cavity suggests perhaps a more direct interaction of the actuator with the boundary before it leaves the nozzle. We see a clear lifting of the boundary layer in Fig. 5, for example. In this section, we compare and constrast mixing layer response to actuation as discussed above with some reduced actuators models that are designed to illuminate the mechanisms.

To estimate the relative importance of the cavity, the jetting and the effect of any thermal heating on the downstream development of the mixing layer, we will consider three other cases. In all three the cavity is removed. In the first, the actuator is placed above the wall, in an experimental configuration for which the plasma appeared to break down as it was advected downstream of the electrodes by the flow.[5] Of course, in the simulation the thermal source does not advect away or break down like an actual plasma. This configuration is shown schematically in Fig. 8(b). In the two other cases, the cavity, which extends from $x = 10\theta_0$ to $x = 20\theta_0$, is replaced with a wall boundary condition (Fig. 8c) with either the wall normal v velocity or both v and temperature T taken from the simulation with the full recessed actuator (Fig. 8a). For this boundary condition actuation, the needed data from the full cavity simulation was saved every 100 time steps and cubic splines were used to interpolate this to provide the time dependent wall bondary conditions. The NSCBCs were used to solve for the density on the wall. The streamwise velocity, u, was set to zero as per the no slip condition. Imposing only v on the wall is loosely thought of as imposing a blowing/suction type of boundary while omitting the effects of heating and the cavity. Prescribing v and T was done to remove the cavity effects but still maintaining the jetting and heating components of the actuation.

(a) basic configuration (b) above wall (c) wall boundary condition on v and/or T

Figure 8. Basic (a) and reduced actuator models (b) and (c).

The momentum thickness of the boundary layer and corresponding downstream mixing layer for all of the simulations is shown in Fig. 9 along with the baseline case. All of the actuated cases spread more than the baseline, but none of the reduced actuators match the spreading caused by the full actuator with the cavity. The case with the actuator above the wall is particularly weak suggesting that the groove geometry is indeed necessary, beyond its role in stabilizing the plasma. The v-only case yields the next weakest response downstream. The mixing layer responds more strongly with both v and T actuation, suggesting some explicit thermal or density role in the subsequent amplification of the disturbances. The cavity-less actuator is seen to be the least effective of all. The fastest spread, however, is for the narrow-cavity case, for which we anticpated improved response based upon the apparently stronger ejection of fluid out of the cavity.

The effect of duty cycle for the full actuator is shown in Fig. 10. We see a minor increase in response with increasing duty cycle, but the mechanisms for this are as yet unclear.

IV.D. Frequency Spectra

While the spreading of the mixing layer is an important measure of its response to the actuation, especially for mixing enhancement efforts, our principal concern is noise reduction which has different objectives. In a related study, adjoint-based methods were used to find optimal actuations for suppressing radiated sound.[26] These did not change the growth of the mixing layer. Instead, it seemed that their principal effect was to organize the flow structures so that they advected with more uniform velocity in the downstream direction. The 20 kHz actuation in the present study is expected to also organize the unsteady flow structures. We assess how the baseline actuator does this and compare the spectral response from this actuator to the reduced actuators.

Figure 11(a) shows the evolution of the pressure spectra downstream for the baseline simulation. There is energy in a broad range of frequencies, but even at $x = 200\theta_0$, most of it is at higher frquencies than

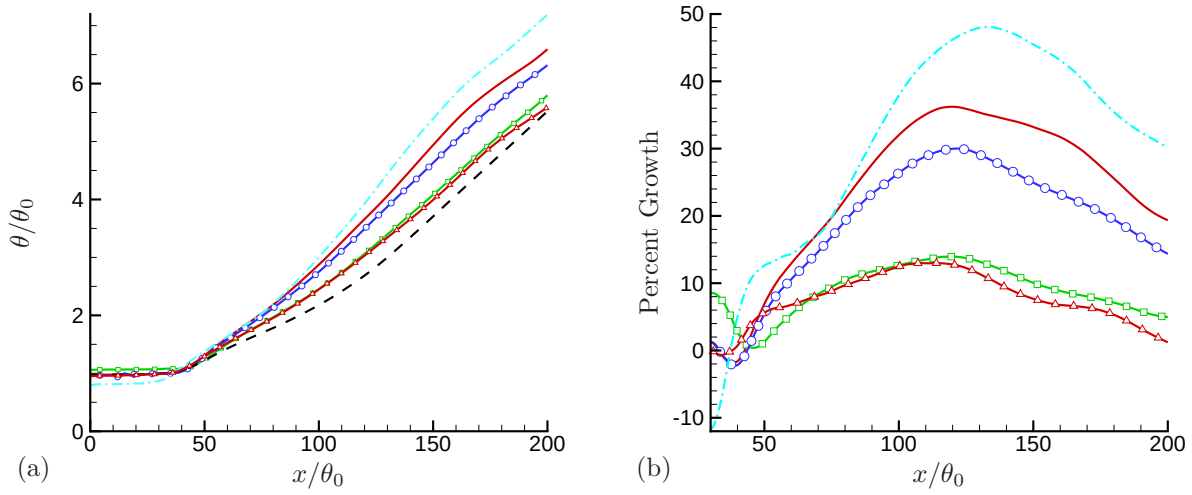

Figure 9. (a) Momentum thickness of the various simulations with and without the cavity. (b) Percent growth of momentum thickness for the simulations with actuation compared to baseline flow. Curves indicate: baseline (– – – –), full cavity simulation (———), no cavity with v imposed (– □ –), no cavity with temperature and v imposed (– ○ –), narrow cavity ($L_c = 5\theta_0$) simulation (— · —), and actuator above wall (– △ –).

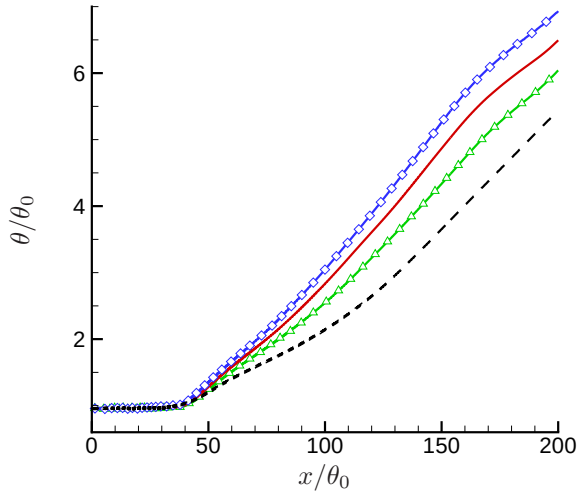

Figure 10. Momentum thickness for simulations with three different duty cycles for the $L_c = 10\theta_0$ cavity: 5% (– △ –), 10% (———), 20% (– ◇ –), and baseline (no acuation) for comparison (– – – –).

20 kHz. The effect of the forcing with the full cavity actuation in Fig. 11(b) is obvious and striking. The flow seems to be nearly perfectly organized into harmonics of the 20 kHz baseline forcing up to 80 kHz. Note, that since the actuation is square-wave like, the nominally 20 kHz signal is indeed stongly dominated by harmonics of this frequency (recall Fig. 3b). Far-field sound has not yet been computed for this flow, but organization like this, without increasing amplitude, is known to suppress noise.[26]

For the v and the v and T boundary condition control cases, the spectral response is very different. The v-only boundary condition control appears to increase amplitudes significantly but fails to organize it into tones, as seen in Fig. 11(c). Adding T input to this, improves organization (Fig. 11d) but nowhere near to the same degree as the cavity actuator control. The reasons for this are unclear. Data not not yet available to conclude if the modes or receptivity of the shear layer above the cavity, say, are needed for the eventual downstream organization of the flow, or if by taking only part of the solution we have inadvertantly excited

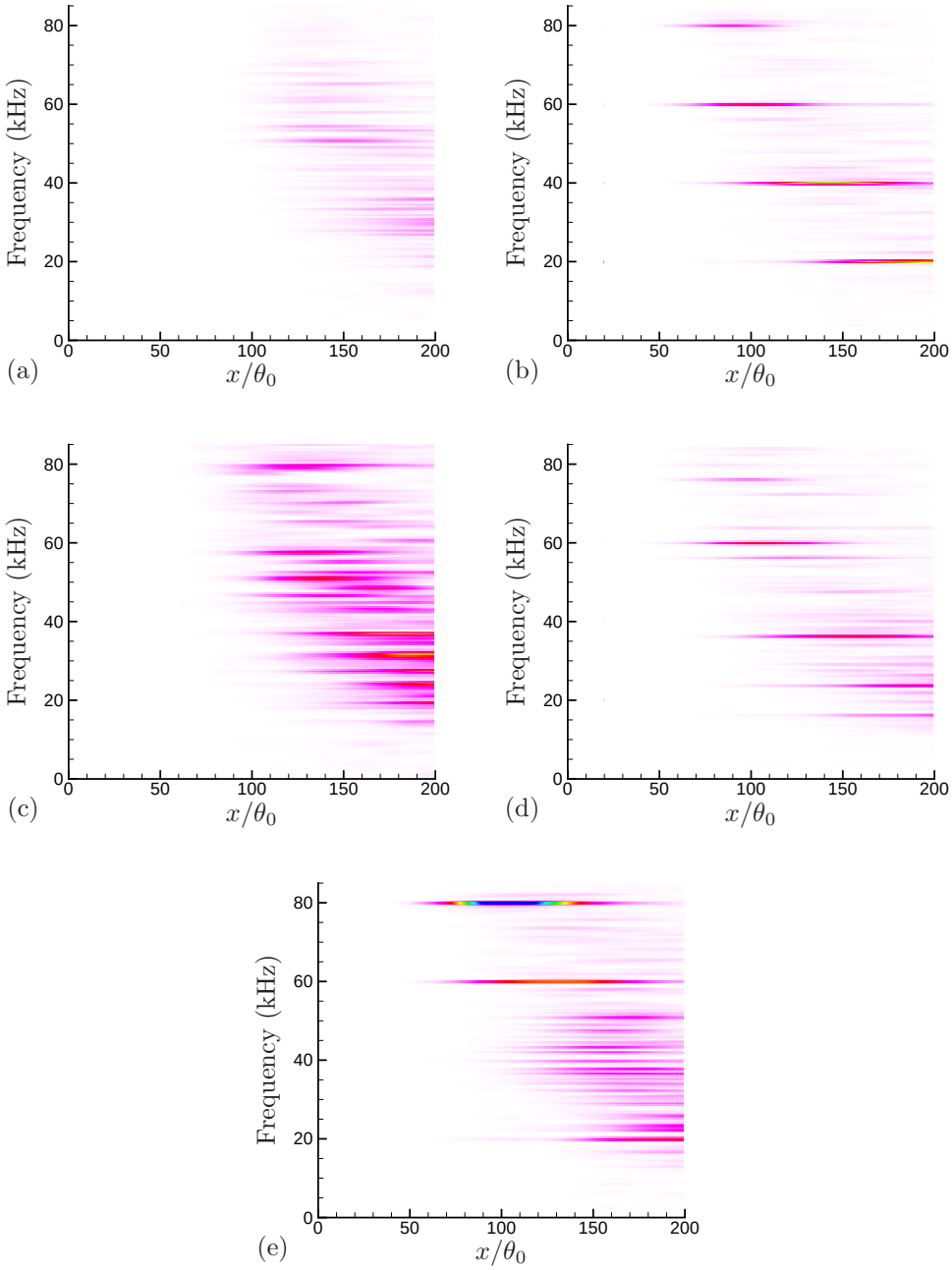

Figure 11. Pressure amplitude along $y = 0$ for the simulations with (a) baseline (no actuation), (b) cavity simulation (10% duty cycle), (c) v prescribed on wall, (d) v and T prescribed on wall, and (e) actuator above wall. Pressure is shown as a function of frequency (in kHz) and streamwise distance.

a broader range of frequencies, which then do not effectively organize the flow downstream. Placing the 'plasma' above the wall without a cavity, excites a stong response in the mixing layer at 80 kHz (Fig. 11e), but the lower frequencies remain broad banded, again supporting the importance of the cavity recess.

For the cavity actuation, which appears to organize the flow into discrete frequencies downstream, it is interesting to track the development of the modes. It is clear in Fig. 12 that all the distrubances grow up slowly from the relatively small perturbation provided by the actuator. For reference, the amplitude of the harmonic frequencies is shown for the the baseline case (Fig. 12a), but it is clear from the scale that they have only a small fraction of the flow's energy. This baseline case also shows highest amplitude for 60 kHz,

which is close to the most unstable frequency (57 kHz) predicted by inviscid parallel-flow linear stability theory.[27]

When actuation is turned on, it is clear when comparing the baseline to the actuated cases that the forcing creates dominant pressure amplitudes at the actuation frequency and its harmonics. The trend shows that as the duty cycle is increased, these frequencies become even stronger in the downstream shear layer region. All four simulations show that the 20 kHz frequency is still growing when the physical domain of the computation ends. The 5% duty cycle case has the strongest 80 kHz harmonic. The 80 kHz tone is shifted downstream and peaks at $x = 100\theta_0$, well before the 10% and 20% cases. The 60 kHz and 80 kHz tones peak at the same location. The 40 kHz data has a relatively weak contribution. As the duty cycle is increased, the progression of growth and subsequent decay of the harmonics with distance from the nozzle exit becomes more as expected in linear stability analysis. Both the 10% and 20% simulations have a steady progression of stronger, lower frequency amplitude peaks as distance from the nozzle exit is increased. The ordering of these harmonics compared to the baseline translates into more efficient spreading (cf. Fig. 10). The higher duty cycle pairing appears to create a more orderly roll-up/pairing of the large structures in the shear layer.

V. Conclusion

In this work we implemented a model for an arc-filament plasma actuator of the kind under development at OSU for jet noise and other types of flow control. The actuator was modeled as a thermal source, which is expected to the principal means by which this type of actuator affects the flow. The overall simulation model included the key features of the flow, including a recessed cavity housing the actuator near the nozzle lip as in the OSU configuration, a detached shear layer above the cavity, and the early stages of mixing layer development downstream of the nozzle lip, but was implemented in two dimensions. It was shown to approximately match both the peak temperature and near-nozzle sound pressure levels measured in the OSU experiments.

Examination of the flow in the neighborhood of the actuator showed that the thermal source causes an expansion that ejects fluid from the recessed cavity in a manner similar to fluidic actuators. A narrower actuator seemed to accentuate this ejection and also gave a stronger response to the forcing downstream.

To better understand the specific means by which the thermal action of the plasma couples with the flow, reduced actuator models were designed that attempted to include different potential mechanisms of its action. Removing the cavity and forcing only the wall-normal velocity or wall-normal velocity and temperature caused some response in the downstream mixing layer, but not to the same degree as the full actuator. Neither of these seemed to organize the downstream flow into tones as successfully as the full actuator. Removing the cavity and placing the plasma model above the wall removed most of its influence on the flow, though it was able to excite a downstream tonal reponse at 80 kHz.

The radiated noise is still under investigation, but the organzation of the flow structures caused by these actuators has previously shown to be an effective means of reducing noise.

Funding from NASA for this work is gratefully acknowledged, including the support of Dr. Jeff Bridges and the supersonic fixed wing program.

References

[1]Corke, T. and Post, M., "Overview of Plasma Actuators: Concepts, Optimization, and Applications," January 2005, AIAA Paper 2005-0563.

[2]Kimmel, R. L., Hayes, J. R., Menart, J. A., and Shang, J., "Effect of Surface Plasma Discharges on Boundary Layers at Mach 5," January 2004, AIAA Paper 2004-0509.

[3]Merriman, S., Ploenjes, E., Palm, P., and Adamovich, I., "Shock Wave Control by Nonequilibrium Plasmas in Cold Supersonic Gas Flows," *AIAA J.*, Vol. 39, No. 8, 2001, pp. 1547–1552.

[4]Samimy, M., Adamovich, I., Webb, B., Kastner, J., Hileman, J., Keshav, S., and Palm, P., "Development and Characterization of Plasma Actuators for High Spee and Reynolds Number Jet Control," *Exp. Fluids*, Vol. 37, No. 4, 2004, pp. 577–588.

[5]Utkin, Y. G., Keshav, S., Kim, J., Kastner, J., Adamovich, I. V., and Samimy, M., "Development and Use of Localized Arc Filament Plasma Actuators for High-Speed Flow Control," *J. Phys. D: Appl. Phys.*, Vol. 40, No. 3, 2007, pp. 685–694.

[6]Samimy, M., Kim, J. H., Kastner, J., Adamovich, I., and Utkin, Y., "Active Control of High-Speed and High-Reynolds-Number Jets Using Plasma Actuators," *J. Fluid Mech.*, Vol. 578, 2007, pp. 305–330.

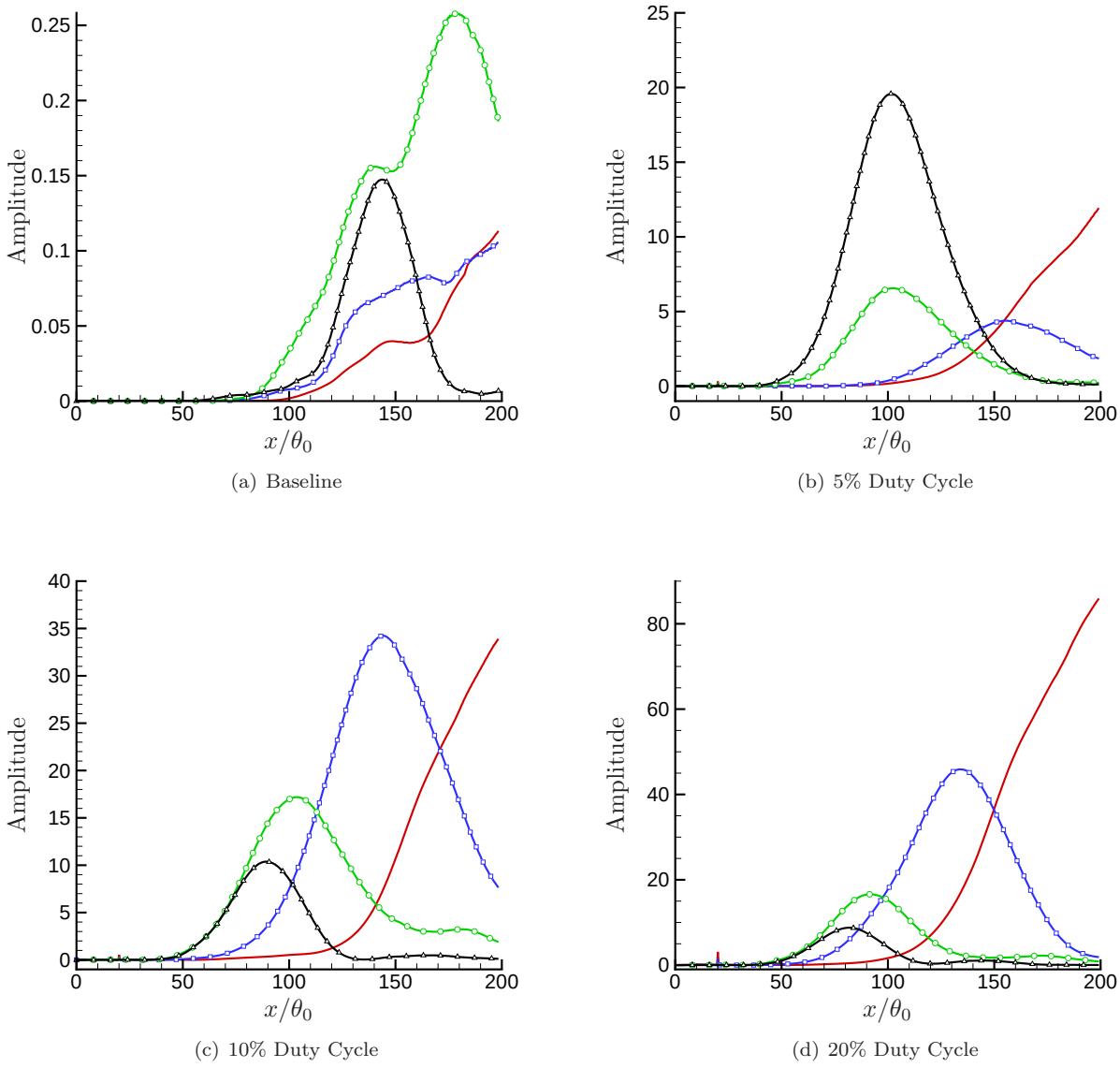

(a) Baseline

(b) 5% Duty Cycle

(c) 10% Duty Cycle

(d) 20% Duty Cycle

Figure 12. Streamwise variation of harmonics of forcing shown by pressure amplitude along $y = 0$ for the cavity simulations with (a) baseline (no actuation), (b) 5% duty cycle, (c) 10% duty cycle, and (d) 20% duty cycle. Curves indicate: 20 kHz (———), 40 kHZ (– □ –), 60 kHz (– ○ –), and 80 kHz (– △ –).

[7]Corke, T. C., Post, M. L., and Orlov, D. M., "SDBD plasma enhanced aerodynamics: concepts, optimization and applications," *Prog. Aero. Sci*, Vol. 43, 2007, pp. 193–217.

[8]Macheret, S. O., Schneider, M. N., and Miles, R. B., "Magnetohydrodynamic and Electrohydrodynamic Control of Hypersonic Flows of Weakly Ionized Plasmas," *AIAA J.*, Vol. 42, 2004, pp. 1378–1387.

[9]Leonov, S., Bityurin, V., Yarantsev, D., and Youriev, A., "The Effect of Plasma Induced Separation," 2003, AIAA Paper 2003-3853.

[10]Samimy, M., Kim, J.-H., Adamovich, I., Utkin, Y., and Kastner, J., "Towards Noise Mitigation in High Speed and High Reynolds Number Jets Using Plasma Actuators," AIAA Paper 2006-2703, May 2006.

[11]Kim, J. H., Adamovich, I., and Samimy, M., "Active Noise Control in a Mach 1.3 Ideally-Expanded Jet with Plasma Actuators," 46th AIAA Aerospace Sciences Meeting and Exhibit, Reno, Nevada, January 2008, AIAA Paper No. 2008-0038.

[12]Shang, J. S., Surzhikov, S. T., Kimmel, R., Gaitonde, D., Menart, J., and Hayes, J., "Mechanisms of Plasma Actuators for Hypersonic Flow Control," *Progress in Aerospace Sciences*, Vol. 41, 2005, pp. 642–668.

[13]Samimy, M., "Preliminary Results on Characterization of LAFPAs," Gas Dynamics and Turbulence Laboratory, The Ohio State University. Internal Document.

[14]Lui, C., *A Numerical Investigation of Shock-Associated Noise*, Ph.D. thesis, Stanford University, 2003.

[15]Kastner, J., Hileman, J., and Samimy, M., "Exploring High-speed Axisymmetric Jet Noise Control using Hartmann Tube Fluidic Actuators," AIAA Paper 2004-0186, January 2004.

[16]Viswanathan, K. and Clark, L. T., "Effect of Nozzle Contour on Jet Aeroacoustics," 42nd AIAA Aerospace Sciences Meeting and Exhibit, Reno, Nevada., January 2004, AIAA Paper No. 2004-0008.

[17]Kleinman, R. R., *On the Turbulence-generated Sound and Control of Compressible Mixing Layers*, Ph.D. thesis, University of Illinois at Urbana-Champaign, Department of Mechanical Science and Engineering, 2009.

[18]Tam, C. and Webb, J., "Dispersion-relation-preserving Finite-difference schemes for Computational Acoustics," *J. Comp. Phys.*, Vol. 107, No. 2, 1993, pp. 262–281.

[19]Lele, S., "Compact Finite-difference Schemes with Spectral-like Resolution," *J. Comp. Phys.*, Vol. 103, No. 1, 1992, pp. 16–42.

[20]Poinsot, T. J. and Lele, S. K., "Boundary-Conditions For Direct Simulations of Compressible Viscous Flows," *J. Comp. Phys.*, Vol. 101, No. 1, 1992, pp. 104–129.

[21]Yoo, C. S. and Im, H. G., "Characteristic Boundary Conditions for Simulations of Compressible Reacting Flows with Multi-dimensional, Viscous and Reaction effects," *Combustion Theory and Modelling*, Vol. 11, No. 2, 2007, pp. 259–286.

[22]Freund, J. B., "Proposed Inflow/Outflow Boundary Condition for Direct Computation of Aerodynamic Sound," *AIAA J.*, Vol. 35, No. 4, 1997, pp. 740–742.

[23]Samimy, M., Kastner, J., Kim, J.-H., Utkin, Y., Adamovich, I., and Brown, C., "Flow and Noise Control in High Speed and High Reynolds Number Jets Using Plasma Actuators," AIAA Paper 2006-2846, June 2006.

[24]Rossiter, J. E., "Wind-tunnel Experiments on the Flow over Rectangular Cavities at Subsonic and Transonic Speeds," NASA Ames Research Center, R&M 3438, October 1964.

[25]Heller, H. H. and Bliss, D. B., "The Physical Mechanisms of Flow-Induced Pressure Fluctuations in Cavities and Concepts for Their Suppression," March 1975, AIAA Paper 1975-491.

[26]Wei, M. J. and Freund, J. B., "A Noise-controlled Free Shear Flow," *J. Fluid Mech.*, Vol. 546, 2006, pp. 123–152.

[27]Michalke, A., "On Spatially Growing Disturbances in an Inviscid Shear Layer," *J. Fluid Mech.*, Vol. 23, 1965, pp. 521–544.